Photodissociation of $BrONO_2$ and N_2O_5: Quantum Yields for NO_3 Production at 248, 308, and 352.5 nm

Matthew H. Harwood, James B. Burkholder,* and A. R. Ravishankara†

Aeronomy Laboratory, National Oceanic and Atmospheric Adminsitration, 325 Broadway, Boulder, Colorado 80303, and Cooperative Institute for Research in Environmental Sciences, University of Colorado, Boulder, Colorado 80309

Received: September 12, 1997; In Final Form: December 1, 1997

Quantum yields for NO_3 production in the photolysis of $BrONO_2$ and N_2O_5 were measured at 248, 308, and 352.5 nm. The measured values for $BrONO_2$ were found to be independent of pressure over the range 150−600 Torr and bath gas (N_2 or O_2) and are 0.28 ± 0.09, 1.01 ± 0.35, and 0.92 ± 0.43 at 248, 308, and 352.5 nm, respectively. Quantum yields of Br and BrO in the photolysis of $BrONO_2$ were also estimated. The measured values for NO_3 production in the photolysis of N_2O_5 were 0.64 ± 0.10, 0.96 ± 0.15, and 1.03 ± 0.15 at 248, 308, and 352.5 nm, respectively. Rate coefficients for the reactions $Br + BrONO_2 \rightarrow Br_2 + NO_3$ (18) and $Cl + BrONO_2 \rightarrow ClBr + NO_3$ (19) were measured at 298 K to be $k_{18} = (6.7 \pm 0.7) \times 10^{-11}$ cm^3 molecule^{-1} s^{-1} and $k_{19} = (1.27 \pm 0.16) \times 10^{-10}$ cm^3 molecule^{-1} s^{-1}. The NO_3 product yields for reactions 18 and 19 were measured to be 0.88 ± 0.08 and 1.04 ± 0.24, respectively. The absorption cross sections for N_2O_5 between 208 and 398 nm are also reported. All quoted uncertainties are 2σ and include estimated systematic errors. On the basis of the measured quantum yields of NO_3, the atmospheric photolysis rate of $BrONO_2$ is discussed.

Introduction

The role of bromine nitrate, $BrONO_2$, as a reservoir for reactive atmospheric bromine is now well established. $BrONO_2$, formed in the reaction between BrO and NO_2, prevents the BrO radical from participating in catalytic cycles involving ClO[1] and HO_x[2] that can destroy ozone. The rates of formation and photodissociation of $BrONO_2$ greatly influence the atmospheric concentration of BrO. $BrONO_2$ also takes part in an ozone destruction cycle. If the photolysis of $BrONO_2$ leads to the formation of NO (without the concomitant production of atomic oxygen) then the following cycle leads to ozone destruction:

$$BrONO_2 + h\nu \rightarrow \rightarrow Br + NO + O_2 \quad (1')$$

$$NO + O_3 \rightarrow NO_2 + O_2 \quad (2)$$

$$Br + O_3 \rightarrow BrO + O_2 \quad (3)$$

$$BrO + NO_2 + M \rightarrow BrONO_2 + M \quad (4)$$

$$\text{Net:} \quad 2O_3 \rightarrow 3O_2$$

Reaction 1′ represents either direct photolysis or a sequence of atmospheric processes where $BrONO_2$ is converted to Br, NO, and O_2. If NO_3 is produced in reaction 1′, its photolysis[3,4] will yield NO:

$$NO_3 + h\nu \rightarrow NO + O_2 \quad (5a)$$

$$\rightarrow NO_2 + O \quad (5b)$$

Modeling studies[5] have shown that, if the atmospheric photolysis of $BrONO_2$ exclusively produces NO_3, the catalytic cycle given above accounts for ∼20% of the ClO_x−BrO_x driven ozone column loss rate (for 1990 chlorine and bromine loadings and for 40° N in the summer). If the NO_3 yield is lower, the contribution of the above cycle to ozone loss will be smaller.

To better assess the role of $BrONO_2$ in the atmospheric chemistry of ozone, it is necessary to determine the photolysis products as a function of wavelength. Several energetically allowed product channels exist

$$BrONO_2 + h\nu \rightarrow BrO + NO_2 \quad \lambda < 1100 \text{ nm} \quad (1a)$$

$$\rightarrow Br + NO_3 \quad \lambda < 900 \text{ nm} \quad (1b)$$

$$\rightarrow Br + NO + O_2 \quad \lambda < 790 \text{ nm} \quad (1c)$$

$$\rightarrow BrONO + O \quad \lambda < 390 \text{ nm} \quad (1d)$$

$$\rightarrow Br + O + NO_2 \quad \lambda < 348 \text{ nm} \quad (1e)$$

$$\rightarrow BrO + NO + O \quad \lambda < 288 \text{ nm} \quad (1f)$$

where the wavelengths given are the thermodynamic thresholds for photolysis for that channel.

In this work, we report quantum yields for NO_3 production, channel 1b, at 248, 308, and 352.5 nm. In the course of this study, quantum yields for NO_3 production in N_2O_5 photolysis at these wavelengths were also measured.

Experimental Section

A known concentration of $BrONO_2$ (determined by UV absorption spectroscopy) was photolyzed by a pulsed excimer laser and the concentration of NO_3 produced was measured as a function of time with a tunable diode laser operating at 661.9

* Author to whom correspondence should be addressed at NOAA/ERL, R/E/AL2, 325 Broadway, Boulder, CO 80303.

† Also associated with the Department of Chemistry and Biochemistry, University of Colorado, Boulder, CO 80309.

S1089-5639(97)02982-4 CCC: $15.00
Published on Web 01/30/1998

nm. The laser fluence was calibrated by photolyzing compounds having known absorption cross sections and photolysis quantum yields. The apparatus used here has been described previously;[6] therefore, only a brief description is given here.

The apparatus consisted of a small volume cell (i.d. = 0.9 cm and 100 cm long) with quartz windows through which $BrONO_2$ or other photolytes diluted in O_2 or N_2 were flowed. Flow rates of gases through the cell were controlled by stainless steel needle valves and measured by electronic mass flowmeters. The total pressure in the cell (monitored using a 1000 Torr capacitance manometer) was varied between 150 and 600 Torr, and the cell temperature was ~298 K.

Photolysis light at 248, 308, and 352 nm from a KrF, XeCl, or XeF excimer laser, respectively, was guided by dielectric mirrors through the cell collinearly with the spectroscopic analysis beam. A D_2 lamp (30 W) was used as the analysis beam to determine the photolyte concentrations. A tunable diode laser (5 mW) nominally operating at 661.9 nm or a xenon arc lamp (75 W) was used to detect the photofragments. In each case, the analysis light sampled only the volume of the reaction cell through which the photolysis beam passed. The deuterium lamp beam exiting the cell was directed onto the slit of a 270 mm focal length spectrograph coupled to a 1024 element diode array detector. The tunable diode laser beam was passed through cutoff filters (ensuring that no photolysis laser light reached the detection optics) and was detected by a red sensitive photodiode. Light from the xenon arc lamp was similarly filtered and passed to a 250 mm focal length monochromator coupled to a photomultiplier tube (PMT).

The diode array spectrograph system was operated with a 100 μm entrance slit yielding a spectral resolution of ~1 nm fwhm over the wavelength range 210 to 350 nm. The minimum measurable absorbance in this system was ~0.001 (*S*:*N* ratio of 1). The monochromator was operated with an entrance slit of 25 μm, giving a spectral resolution of 0.14 nm, fwhm, and was used to measure transient absorption at specific wavelengths. The minimum detectable absorbance changes in the monochromator/PMT system for a typical integration (averaging 50 waveforms) was 0.001 (*S*:*N* ratio of 1). The wavelength scales of the monochromator and spectrometer were calibrated using the emission from a low-pressure mercury pen-ray lamp. The wavelength of the tunable diode laser was measured with the monochromator/PMT system. The high stability of the tunable diode laser allowed absorbance changes of 5×10^{-5} to be measured (*S*:*N* ratio of 1).

Materials. The carrier gases used were O_2 (UHP) and N_2 (UHP). $BrONO_2$ was produced by the reaction of BrCl with $ClONO_2$.[5,7] The $BrONO_2$ flow into the cell was regulated by passing a flow of carrier gas over the $BrONO_2$ sample held at temperatures in the range 200−230 K. Ozone (prepared by passing O_2 through an ozonizer and trapping the O_3 onto silica gel at 195 K) and N_2O_5 (prepared by the reaction between O_3 and NO_2 and stored at 195 K) were delivered to the reaction cell by passing the carrier gas over the compounds. HNO_3 was prepared by passing the carrier gas over a 3:1 mixture of concentrated H_2SO_4 and HNO_3 held at 273 K. F_2 (5% in He) and Cl_2 (6.4% in He) were used as supplied.

Method. NO_3 Quantum Yields in $BrONO_2$ Photolysis. The amount of NO_3 produced in the photolysis of $BrONO_2$ under optically thin conditions is given by the following expression

$$\Delta[NO_3] = [BrONO_2]\,\sigma_\lambda(BrONO_2)\,\Phi_\lambda^{NO_3}(BrONO_2)\,F(\lambda) \quad \text{(I)}$$

where $F(\lambda)$ is the photolysis fluence (photon cm^{-2} $pulse^{-1}$) at wavelength λ, $\sigma_\lambda(BrONO_2)$ is the $BrONO_2$ absorption cross section (cm^2 $molecule^{-1}$) and $\Phi_\lambda^{NO_3}(BrONO_2)$ is the quantum yield for NO_3 production at the photolysis wavelength. The photolysis fluence was calibrated by photolyzing N_2O_5 and measuring the concentration of NO_3 produced; it is given by the expression

$$\Delta[NO_3] = [N_2O_5]\,\sigma_\lambda(N_2O_5)\,\Phi_\lambda^{NO_3}(N_2O_5)\,F(\lambda) \quad \text{(II)}$$

where $\sigma_\lambda(N_2O_5)$ and $\Phi_\lambda^{NO_3}(N_2O_5)$ are the N_2O_5 absorption cross section and quantum yield for NO_3 production at the photolysis wavelength, respectively. Combining expressions I and II and relating the concentrations of NO_3 to measured absorbances, $\Delta A_{NO_3}(N_2O_5)$, and $\Delta A_{NO_3}(BrONO_2)$, leads to the following expression for the NO_3 quantum yield:

$$\Phi_\lambda^{NO_3}(BrONO_2) = \frac{\Delta A_{NO_3}(BrONO_2)\,[N_2O_5]\,\sigma_\lambda(N_2O_5)\,\Phi_\lambda^{NO_3}(N_2O_5)}{\Delta A_{NO_3}(N_2O_5)\,[BrONO_2]\,\sigma_\lambda(BrONO_2)} \quad \text{(III)}$$

The $BrONO_2$ and N_2O_5 concentrations in the cell were both determined by UV absorption. Absorption cross sections of Burkholder et al.[5] ($BrONO_2$) and Harwood et al.[8] (N_2O_5) were used to fit the measured absorption spectra to determine the concentrations. NO_3 has a strong broad absorption band peaking at 661.9 nm ($\sigma_{max} = 2.23 \times 10^{-17}$ cm^2 $molecule^{-1}$).[6] The tunable diode laser was tuned to the peak to obtain maximum sensitivity for detecting NO_3. The exact value of the NO_3 absorption cross section is not required in the analysis (see eq III).

The various absorption cross sections and quantum yields used in the data anaylsis in this study are listed in Table 1.

TABLE 1: Absorption Cross Sections Used in This Study

species	cross section (10^{-20} cm^2 $molecule^{-1}$) 248 nm	308 nm	352.5 nm	other	ref
$BrONO_2$	89.0	14.7	6.41		5
N_2O_5	41.9	2.40	1.89		this work
O_3		13.6		$\sigma_{265.54nm} = 965$ $\sigma_{253.7nm} = 1150$	9
HNO_3	2.0				10
Cl_2			18.1		9
ClO				$\sigma_{253.7\,nm} = 3.93$	9
NO_3				$\sigma_{661.9\,nm} = 2230$	6
Br_2			4.39		11
F_2[a]	$\alpha = 0.64$	$\alpha = 0.87$	$\alpha = 0.32$		this work

[a] α is the ratio of the F_2 cross section at the wavelength given to that at the peak of the absorption spectrum ($\sigma_{Peak} = 2.47 \times 10^{-20}$ cm^2 $molecule^{-1}$ [12]).

NO_3 Quantum Yields in N_2O_5 Photolysis. Our measured NO_3 quantum yield in the photolysis of $BrONO_2$ is dependent on the NO_3 quantum yield from N_2O_5 photolysis. Therefore, we have measured the NO_3 quantum yield in the photolysis of N_2O_5. Quantum yields of NO_3 in N_2O_5 photolysis, $\Phi_\lambda^{NO_3}(N_2O_5)$, have been measured previously at selected wavelengths between 248 and 350 nm (DeMore et al.[9] and references therein). However, it has not been measured between 300 and 340 nm, the important actinic region for the lower stratosphere and the troposphere. In this study the NO_3 quantum yield was measured relative to four actinometric standards. These approaches are described below for the different wavelengths used.

(a) Photolysis of HNO_3 (248 nm). This method utilized the photolysis of HNO_3 followed by the reaction of the OH photofragment with HNO_3 to produce NO_3

$$HNO_3 + h\nu \rightarrow OH + NO_2 \quad (6)$$

$$OH + HNO_3 \rightarrow H_2O + NO_3 \quad (7)$$

HNO_3 concentrations were sufficiently high ($>1 \times 10^{17}$ molecule cm^3) to ensure that the production of NO_3 was essentially complete in 50 μs. The change in the NO_3 concentration is given by the expression

$$\Delta[NO_3] = [HNO_3]\, \sigma_\lambda(HNO_3)\, \Phi_\lambda^{OH}(HNO_3)\, F(\lambda)\, \Phi_{Rx}^{NO_3}(7) \quad \text{(IV)}$$

The quantum yield for OH production in the photolysis of HNO_3, $\Phi_\lambda^{OH}(HNO_3)$, and the NO_3 yield from reaction 7, $\Phi_{Rx}^{NO_3}(7)$, were both taken to be unity.[9]

(b) Photolysis of F_2/HNO_3 Mixtures (248, 308, and 352.5 nm). The photolysis of F_2 followed by the reaction of F with HNO_3 constituted another actinometric method:

$$F_2 + h\nu \rightarrow 2F \quad (8)$$

$$F + HNO_3 \rightarrow HF + NO_3 \quad (9)$$

The concentrations of F_2, $(1-10) \times 10^{17}$ molecule cm^{-3} , and HNO_3, $(1-5) \times 10^{15}$ molecule cm^{-3}, were such that the concentration of HNO_3 that was photolyzed was negligible compared to the concentration of F atoms that was produced. Reaction 9 was always greater than 90% complete within 85 μs and often in less than 20 μs, $k_9 = 2.3 \times 10^{-11}$ cm^3 molecule^{-1} s^{-1}. The change in the NO_3 concentration is given by

$$\Delta[NO_3] = [F_2]\, \sigma_\lambda(F_2)\, \Phi_\lambda^{F}(F_2)\, F(\lambda) \quad \text{(V)}$$

The quantum yield for F atom production, $\Phi_\lambda^{F}(F_2)$, was taken to be 2.

(c) Photolysis of Ozone (308 nm). Ozone was photolyzed, and the increase in the transmitted light at 265.5 nm was measured with the monochromator/PMT system:

$$O_3 + h\nu \rightarrow O_2 + O \quad (10)$$

The change in ozone concentration is given by

$$\Delta[O_3] = [O_3]\, \sigma_\lambda(O_3)\, \Phi_\lambda^{O}(O_3)\, F(\lambda) \quad \text{(VI)}$$

The quantum yield for O atom production in O_3 photolysis, $\Phi_\lambda^{O}(O_3)$, was taken to be unity. To calculate the NO_3 quantum yields from N_2O_5 photolysis, equations II and VI are combined but the changes in absorbances of two different molecules, i.e., O_3 and NO_3, are needed. Therefore, the absolute absorption cross section of O_3 and NO_3 are needed for this method.

(d) Photolysis of Cl_2/O_3 Mixtures (352.5 nm). Cl_2 was photolyzed in the presence of O_3, and the increase in the transmitted light at 253.7 nm was measured with the monochromator/PMT system.

$$Cl_2 + h\nu \rightarrow 2Cl \quad (11)$$

$$Cl + O_3 \rightarrow O_2 + ClO \quad (12)$$

Each Cl atom removes one O_3 molecule and produces one ClO radical. The Cl atom concentration is given as

$$\Delta[Cl] = \frac{\Delta A(253.7\text{ nm})}{(\sigma_{253.7}(O_3) - \sigma_{253.7}(ClO))L} = [Cl_2]\, \sigma_\lambda(Cl_2)\, \Phi_\lambda^{Cl}(Cl_2)\, F(\lambda) \quad \text{(VII)}$$

where L is the absorption path length and the Cl atom quantum yield in Cl_2 photolysis, $\Phi_\lambda^{Cl}(Cl_2)$, was taken to be 2.

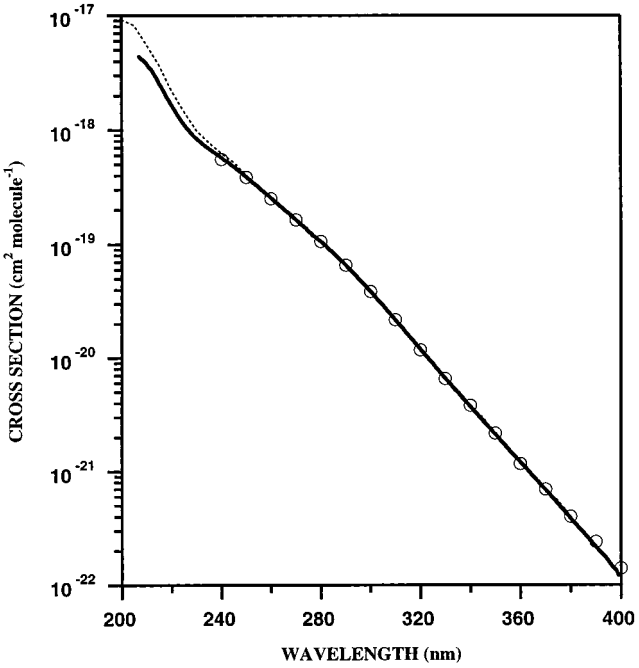

Figure 1. Comparison of N_2O_5 absorption spectra measured here with those from previous studies: solid line, this work; dashed line, DeMore et al.;[9] open circles, Harwood et al.;[8] The discrepancies between these reported values are discussed in the text.

Results

The quantum yield for NO_3 production in $BrONO_2$ photolysis was measured relative to that from N_2O_5 at the same wavelength. Therefore, the NO_3 quantum yield in N_2O_5 results are presented first followed by the results from our studies of $BrONO_2$ photolysis.

N_2O_5 Photolysis. N_2O_5 concentrations were determined by absorption in the 240−300 nm region before and after a pulsed photolysis measurement. The concentration varied by <5% over the course of the measurements and was averaged for data analysis.

The N_2O_5 absorption spectrum measured with the diode array spectrometer showed systematic differences from that recommended by DeMore et al.[9] at wavelengths shorter than 250 nm. Figure 1 compares the spectrum measured here with that recommended by DeMore et al. and the recently reported measurements by Harwood et al.[8] Our spectrum is normalized to the value reported by Harwood et al. at 280 nm. Our cross sections are systematicaly lower than that recommended by DeMore et al. below 260 nm while it is in excellent agreement at longer wavelengths. It agrees well with the data of Harwood et al., ±3%, over the entire wavelength range of overlap. Our N_2O_5 spectra were recorded using two separate diode array systems and three different N_2O_5 samples. All measured spectra were in excellent agreement. A possible reason for the discrepancy at short wavelengths could be contributions to the

TABLE 2: N_2O_5 Absorption Cross Sections

wavelength (nm)	σ^a	wavelength (nm)	σ	wavelength (nm)	σ
208	418	272	14.9	336	0.462
210	380	274	13.7	338	0.412
212	335	276	12.4	340	0.368
214	285	278	11.4	342	0.328
216	236	280	10.5	344	0.293
218	196	282	9.59	346	0.262
220	165	284	8.74	348	0.234
222	140	286	7.94	350	0.210
224	119	288	7.20	352	0.188
226	105	290	6.52	354	0.167
228	92.6	292	5.88	356	0.149
230	83.8	294	5.29	358	0.133
232	76.9	296	4.75	360	0.120
234	70.8	298	4.26	362	0.107
236	65.8	300	3.81	364	0.0958
238	61.4	302	3.40	366	0.0852
240	57.1	304	3.03	368	0.0763
242	53.1	306	2.70	370	0.0685
244	49.3	308	2.40	372	0.0613
246	45.6	310	2.13	374	0.0545
248	41.9	312	1.90	376	0.0484
250	38.6	314	1.68	378	0.0431
252	35.5	316	1.49	380	0.0383
254	32.6	318	1.33	382	0.0341
256	29.9	320	1.18	384	0.0305
258	27.5	322	1.05	386	0.0273
260	25.2	324	0.930	388	0.0242
262	23.1	326	0.826	390	0.0215
264	21.1	328	0.735	392	0.0193
266	19.4	330	0.654	394	0.0172
268	17.8	332	0.582	396	0.0150
270	16.2	334	0.518	398	0.0134

[a] Units of 10^{-20} cm^2 molecule^{-1}.

measured absorption from an HNO_3 impurity in previous studies. A mass spectrometric analysis of our samples using chemical ionization showed that they contained less than 1% HNO_3. An HNO_3 impurity at this level would make a negligible contribution to the N_2O_5 spectrum. As a further test, N_2O_5 spectra recorded after flowing the gas through or around a trap packed with Nylon were identical. Nylon has been shown to efficiently scrub HNO_3 out of a gas stream.[12] We use the cross sections measured in this study, which are listed in Table 2.

A typical NO_3 absorption profile (at 661.9 nm) following N_2O_5 photolysis is shown in Figure 2a. The appearance of NO_3 was essentially instantaneous on the time scale of the measurements (<10 μs). When pure N_2O_5 (no bath gas) was photolyzed, the appearance of the NO_3 was delayed, as observed previously.[13] The delayed appearance is consistent with the quenching of vibrationally and electronically exited NO_3 to the detected ground state. We measured an effective second-order rate coefficient of $k_{13} = (1.8 \pm 0.4) \times 10^{-11}$ cm^3 molecule^{-1} s^{-1} for the quenching of NO_3 by N_2O_5 produced from 248 nm photolysis of N_2O_5

$$N_2O_5 + NO_3^* \rightarrow N_2O_5 + NO_3 \qquad (13)$$

(where NO_3* indicates energetically excited NO_3 which is not detected spectrospcopically at 661.9 nm). To rapidly quench NO_3*, we used 150−700 Torr of N_2 bath gas. Torabi[13] reported the effective rate coefficient for quenching of NO_3* (formed from N_2O_5 photolysis) by N_2 to be 1.6×10^{-13} cm^3 molecule^{-1} s^{-1}. In 150 Torr of N_2, the quenching of excited NO_3 should be complete within 5 μs. As a further check, the absorption profile of NO_3 (following 308 nm photolysis of N_2O_5) was monitored at both 661.9 and 657.2 nm (on and off the NO_3 absorption peak). The ratio of the measured absorptions at the two wavelenghs (under identical experimental conditions) was in agreement with the ratio of the room temperature NO_3 absorption cross sections at these two wavelengths.

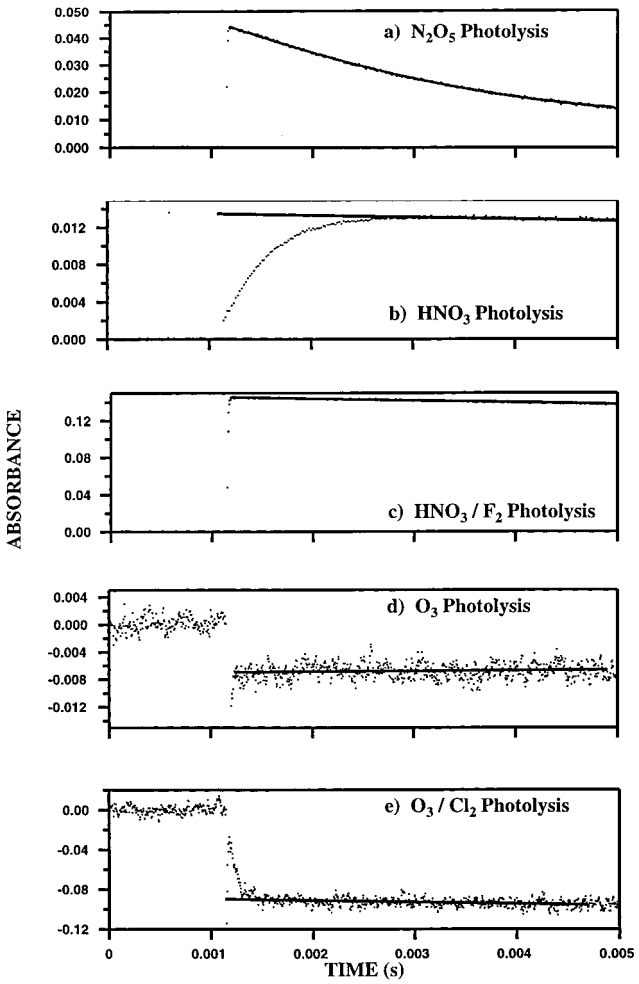

Figure 2. Representative temporal absorption profiles measured for the various actinometeric methods and photolysis wavelengths: (a) N_2O_5 photolysis at 248 nm, NO_3 absorption at 661.9 nm; (b) HNO_3 photolysis at 248 nm followed by reaction 7, NO_3 absorption at 661.9 nm; (c) F_2 photolysis at 308 nm followed by reaction 9, NO_3 absorption at 661.9 nm; (d) O_3 photolysis at 308 nm, O_3 absorption at 265 nm; (e) Cl_2 photolysis at 352.5 nm followed by reaction 12, absorption at 253.6 nm.

After its photolytic production, NO_3 decayed slowly with a first-order rate coefficient that is consistent with NO_3 removal through reaction with NO_2 (present in the $N_2O_5 \leftrightarrow NO_2 + NO_3$ equilibrium) and/or NO (an NO_2 photolysis product). The initial NO_3 absorption was determined by linear extrapolation to the time of the laser pulse. The extrapolation accounted for less than a 2% increase in the NO_3 signal. Plots of the initial NO_3 absorption versus $[N_2O_5]$ were found to be linear with zero intercepts within the precision of the measurements.

The concentrations of the other species used in the fluence calibrations were also determined by UV spectroscopy. Literature absorption cross section data were used to fit the measured absorption spectra. In the case where two or more absorbers were present, linear least-squares fitting was used to fit the absorption cross sections to the measured absorption spectrum and, hence, to determine the concentrations of both species. In all experiments the precursor concentrations were measured before and after photolysis and the concentrations were found to be stable to within 5%.

TABLE 3: Quantum Yields for NO_3 Production in N_2O_5 Photolysis[a]

	NO_3 quantum yield		
calibration method	248 nm	308 nm	352.5 nm
HNO_3 photolysis	0.67 ± 0.14		
HNO_3/F_2	0.64 ± 0.08	0.88 ± 0.10	0.91 ± 0.04
O_3 photolysis		1.03 ± 0.10	
O_3/Cl_2			1.21 ± 0.04
value used in $BrONO_2$ analysis	0.64	1.0	1.0

[a] The quoted uncertainties are 2σ of the measurement precision. The absolute uncertainties (2σ) including estimated errors are ±15% of the measured value.

Figure 2b−e shows the temporal profiles for the species monitored during the laser fluence calibrations described above. Figure 2b shows the NO_3 production following HNO_3 photolysis. A slow, $<50\ s^{-1}$, first-order removal of NO_3 was observed in these experiments (possibly due to the NO_2 impurity in the HNO_3). Using numerical fitting of the observed absorption traces, the concentration of NO_3 lost through this process was determined. The calculated N_2O_5 quantum yields were corrected (<4%). Figure 2c displays NO_3 production following the reaction of F atoms with HNO_3, and Figures 2d and 2e show the absorption measured at 265.54 (O_3) and 253.7 ($ClO + O_3$) nm, respectively. In all cases the measured change in absorption was found to be proportional to the precursor concentration.

The quantum yields at all three wavelengths for NO_3 production following N_2O_5 photolysis are given in Table 3. The quantum yield values were independent of pressure. The values used in analyzing NO_3 quantum yields from $BrONO_2$ photolysis are also given.

Quantum Yields in $BrONO_2$ Photolysis. Freshly prepared $BrONO_2$ samples contained OClO, Br_2, and Br_2O impurities. These impurities were detected by their UV/visible absorption. After pumping on the samples at 200−210 K, the OClO impurity was reduced to undetectable levels ($<5 \times 10^{11}$ molecule cm^{-3}). The Br_2 concentrations were typically <5% of the amount of $BrONO_2$. However, Br_2O was present in varying amounts in all measurements. When large concentrations of $BrONO_2$ ($>5 \times 10^{14}$ molecule cm^{-3}) were used, the Br_2O levels were below 1%. At lower $BrONO_2$ concentrations, the Br_2O made up a larger fraction of the reaction mixture but was always <10%. These observations are consistent with the formation of Br_2O via the heterogeneous reaction of $BrONO_2$ with a water impurity followed by decomposition of HOBr. The concentrations of $BrONO_2$ and Br_2O were determined spectroscopically by fitting the absorption spectra[5,14] of both species to the measured aborption spectrum. The $BrONO_2$ concentrations were stable to within 10% over the course of a measurement, though the Br_2O concentrations changed more, often by a factor of 2. As with the other measurements, the concentrations of $BrONO_2$ and Br_2O were determined before and after each photolysis run and the average value was used.

Typical temporal profiles of NO_3 absorption observed upon photolysis of $BrONO_2$ at 248, 308, and 352.5 nm are shown in Figure 3a−c. In each case, there is an instantaneous rise in the NO_3 absorption upon photolysis which is followed by a slower first-order rise in its concentration. The first-order rate coefficient, k', for the production of NO_3 was determined from

$$\ln(A_\infty(NO_3) - A_t(NO_3)) = k't \qquad \text{(VIII)}$$

where $A_\infty(NO_3)$ is the absorption when the NO_3 production is complete. This rate coefficient was found to be proportional to the $BrONO_2$ concentration and independent of the cell pressure. Extrapolation of the NO_3 signal according to eq VIII to the time of the laser pulse yielded the concentration of photolytically generated NO_3. The post-photolysis NO_3 profile is consistent with the formation of NO_3 by photolysis followed by the reaction of one or more photoproducts with $BrONO_2$ to yield NO_3.

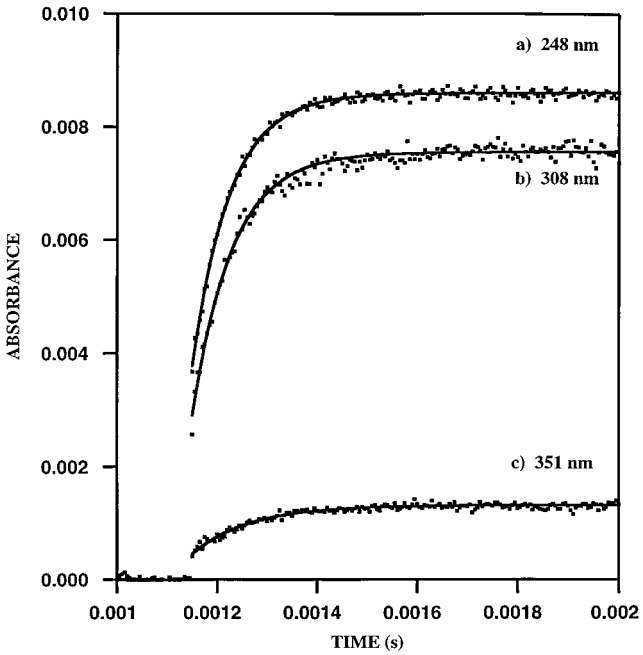

Figure 3. NO_3 temporal absorption profiles measured following excimer laser photolysis of $BrONO_2$ at (a) 248 nm, (b) 308 nm, and (c) 352.5 nm. The solid lines are fits to the data (see text) and were used to determine the primary photolysis quantum yields.

$$BrONO_2 + h\nu \rightarrow Br + NO_3 \qquad \text{(1b)}$$

$$BrONO_2 + X \rightarrow XBr + NO_3 \qquad \text{(14)}$$

X could come from the photolysis of $BrONO_2$ (potentially, X = Br or O) or from the photolysis of the impurities Br_2O or Br_2:

$$Br_2O + h\nu \rightarrow BrO + Br \qquad \text{(15a)}$$

$$\rightarrow Br + O + Br \qquad \text{(15b)}$$

$$Br_2 + h\nu \rightarrow Br + Br \qquad \text{(16)}$$

where channel 15b is energetically possible only below 340 nm. The formation of NO_3 via reactions of photolysis products was unavoidable and contributed to the uncertainty in determining the photolysis quantum yield. Br atoms, which react rapidly with $BrONO_2$ (see below) are a coproduct of NO_3, reaction 1b. Several potential Br atom scavengers were tried (C_2H_2, C_2H_4). However, $BrONO_2$ reacted rapidly (either heterogeneously or in the gas phase) with these organic compounds and prevented such measurements. Therefore, a secondary rise of at least the same magnitude as the initial NO_3 signal was expected. As shown in Figure 3, the signal due to the secondary rise at each of the photolysis wavelengths is greater than that from the primary photolysis. In some experiments an excess of O_2 was added to scavange photolytically produced O atoms through the reaction

$$O + O_2 + M \rightarrow O_3 + M \qquad \text{(17)}$$

TABLE 4: Quantum Yield of NO_3 in the Photolysis of $BrONO_2$[a]

photolysis wavelength (nm)	number of measurements	$[BrONO_2]$ range/ 10^{14} molecule cm^{-3}	quantum yield
248	36	0.5−5.0	0.28 ± 0.09
308	27	0.5−5.0	1.01 ± 0.35
352.5	40	0.5−5.0	0.92 ± 0.43

[a] The quoted absolute uncertainties are 2σ and include estimated systematic errors.

Only in the 248 nm photolysis experiments did the addition of O_2 have any affect on the total NO_3 signal. In all cases, the photolytically produced NO_3, as opposed to that produced via reaction, was well defined and was due only to photolysis of $BrONO_2$.

To determine the quantum yield for channel 1b, the change in the absorption due to the NO_3 produced by photolysis, $\Delta A_P(NO_3)$, was determined by extrapolation of the measured NO_3 temporal profile as described above. The $BrONO_2$ concentrations were kept sufficiently low ($< 5 \times 10^{14}$ molecule cm^{-3}) to separate in time the photolytic production from that due to reaction 14. The value of $\Delta A_P(NO_3)$ determined using this graphical method was compared to the result from a numerical fitting approach. In the numerical approach, the rate equations for reactions 1b and 14 were numerically integrated and compared with the observed profiles. Absorption due to NO_3 produced by reaction 14, $\Delta A_R(NO_3)$, along with $\Delta A_P(NO_3)$ and the first-order rate coefficient for the reactive production were varied to best fit the observed profile. The results from the two different analysis methods agreed to within 5%. The determination of the quantum yield for channel 1b is most difficult at the longer photolysis wavelengths (352.2 nm), where the concentration of NO_3 produced is low, due to the smaller $BrONO_2$ absorption cross sections and low concentrations of $BrONO_2$ that were used. The $BrONO_2$ concentration cannot be raised to increase the signal because it would prevent us from separating process 1b from 14 in time.

The value of $\Delta A_P(NO_3)$ determined in the graphical approach was used in eq III to calculate the quantum yield of channel 1b, $\Phi(1b)$, at the three photolysis wavelengths. In all sets of experiments, plots of $\Delta A_P(NO_3)$ versus $[BrONO_2]$ were found to be linear with a zero intercept. The results obtained for each photolysis wavelength are described separately below.

248 nm Photolysis. The quantum yield for channel 1b at 248 nm was measured to be 0.28 ± 0.06 in both N_2 and O_2 bath gases. The results are given in Table 4 and plotted in Figure 4a as a function of pressure. Each point in Figure 4a represents the average of 2−7 individual $BrONO_2$ photolysis measurements with 4−8 N_2O_5 calibrations. The error bars shown in the figure represent the measurement precision (2σ). The quantum yield shows no statisticaly significant trend with pressure.

The rise of NO_3 following photolysis was expected to be mainly due to the reaction of $BrONO_2$ photofragments with $BrONO_2$. The amount of Br_2O photolyzed was always less than 5% of that of $BrONO_2$. The Br_2 photolysis was negligible. The NO_3 yield due to the sum of photolytic and reactive production, $\Phi_\infty(NO_3)$, was determined to be 1.12 ± 0.11 in N_2 and 0.91 ± 0.18 in excess O_2. These two yields are almost the same, and the difference between the two, ~0.2, may not be statistically significant; this difference, if real, may be due to O atom production in the 248 nm photolysis of $BrONO_2$.

Production of BrO was monitored by using the monochromator/PMT system (150 μm slits, fwhm = 0.35 nm) on both the (7,0), 338.2 nm, and (4,0), 354.7 nm, absorption bands of BrO. The yields were measured in an excess of O_2, 600 Torr, to suppress BrO formation from O atom reactions with $BrONO_2$ and Br_2O. BrO was produced immediately upon photolysis with no subsequent formation of BrO due to other reactions. Using the BrO cross sections of 1.6×10^{-17} cm^2 $molecule^{-1}$ and 0.8×10^{-17} cm^2 $molecule^{-1}$ for the (7,0) and (4,0) absorption bands, respectively, the ratio of the photolytically produced BrO to NO_3 was determined. The measured ratio showed considerable scatter due to our low sensitivity for detecting BrO and the changing amounts of the Br_2O impurity. It ranged from 1.2 to 2.2 with an average value of $\Delta A_P[BrO]/\Delta A_P[NO_3] = 1.8 \pm 0.7$.

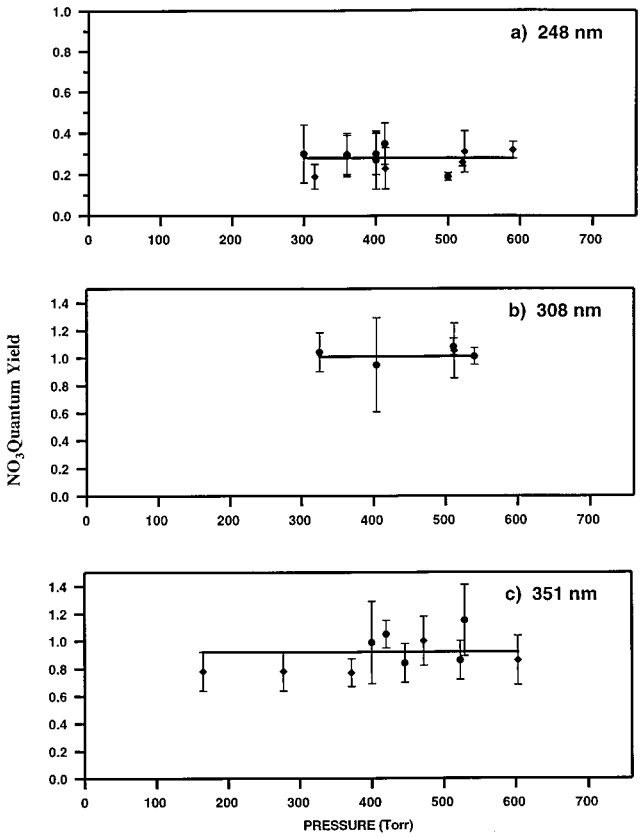

Figure 4. NO_3 quantum yields in $BrONO_2$ photolysis as a function of pressure at (a) 248 nm, (b) 308 nm, and (c) 352.5 nm. The error bars are the 2σ uncertainties of the measurements. The solid lines represent the average value of the data (see Table 4).

308 nm Photolysis. The NO_3 profiles recorded following photolysis of $BrONO_2$ at 308 nm showed the same features as those at 248: an initial jump followed by a slower formation of NO_3 with a first-order rate coefficient proportional to $[BrONO_2]$. The results are given in Table 4 and plotted in Figure 4b as a function of pressure. Again, no pressure or bath gas dependence was observed. The average value of $\Phi(1b)$ was 1.01 ± 0.10 (2σ).

The rate coefficient for NO_3 formation was similar to that observed in the 248 nm photolysis (see below). However, the yield of NO_3 due to photolysis of $BrONO_2$ and reaction 14 varied between 2.6 and 3.3 with an average value of 2.9 ± 0.3. This is above the value of 2 expected for $\Phi_\infty(NO_3)$ if $\Phi(1b)$ is unity as suggested from our results. We attribute the larger yield to photolysis of Br_2O, which has a significant absorption cross section at this wavelength. The Br_2O absorption at 308 ranged between 20% and 160% of that due to $BrONO_2$. Thus, it is likely that NO_3 was being produced through the reaction of Br_2O photofragments with $BrONO_2$. $\Phi_\infty(NO_3)$ showed a slight correlation with $[Br_2O]$ but this was difficult to quantify

because the $[Br_2O]$ varied considerably during each measurement. In addition, at high $[Br_2O]$, Br atoms might react with Br_2O rather than $BrONO_2$. $\Phi_\infty(NO_3)$ was measured in N_2 and O_2 under identical conditions (similar Br_2O levels) and its value was found to be systematically higher in excess N_2. If $\Phi(1b) = 1$ and reaction 14 (with X = Br or O) gives NO_3 with 100% efficiency, then the "extra" NO_3 (presumed due to Br_2O photolysis) is 1.3 times greater in N_2 than in O_2. This observation implies O atom formation in the photolysis of Br_2O.

In several experiments, the BrO yield was measured by monitoring its 4-0 band to be <0.27. This assumes that BrO is not produced in Br_2O photolysis. However, if, as we expect, there are other sources of BrO (reaction 15a and reaction of Br with Br_2O) the BrO yield in $BrONO_2$ photolysis will be much smaller.

352.5 nm Photolysis. A typical temporal profile of NO_3 in the $BrONO_2$ photolysis at 352.5 nm is shown in Figure 3c. Again the photolytic and kinetic production of NO_3 are clearly separate. However, because of the low NO_3 absorption signals, the uncertainty in determining $\Delta A_P(NO_3)$ is rather large. The measured quantum yields for channel 1b are given in Table 4 and shown in Figure 4c as a function of carrier gas pressure. As there is no statistical pressure or bath gas dependence to the quantum yield, we report the average of all measurements $\Phi(1b) = 0.92 \pm 0.14$. In these experiments, the Br_2O absorption at 352.5 nm ranged between 2 and 4 times that of $BrONO_2$ absorption (the ratio of the Br_2O absorption cross section to that of $BrONO_2$ increases at the longer wavelengths) and, thus, much of the post photolysis rise of NO_3 may be due to the reaction of Br_2O photoproducts with $BrONO_2$. $\Phi_\infty(NO_3)$ ranged between 2.8 and 5 times the photolytic NO_3 yield.

Kinetic Measurements. As noted above, a significant amount of NO_3 was produced by the reaction of a $BrONO_2$ (or Br_2O) photoproduct with $BrONO_2$. The rate coefficient for this reaction is a clue to the identity of the photoproduct, which will be either Br or O atoms. Therefore, the rate coefficient for the reaction of Br with $BrONO_2$ at room temperature

$$Br + BrONO_2 \rightarrow Br_2 + NO_3 \qquad (18)$$

was measured. A mixture of $BrONO_2$ and Br_2 was photolyzed at 352.5 nm (XeF excimer laser) under conditions which ensured that the amount of $BrONO_2$ photolyzed was negligible relative to that of Br_2. The $BrONO_2$ concentration was varied over the range $(1.4-15) \times 10^{13}$ molecule cm^{-3}, and the Br_2 concentration was in the range (1.7 to 6.5) $\times 10^{15}$ molecule cm^{-3}. Approximately 150 Torr of He was used as the buffer gas. The production of NO_3 was measured under pseudo-first-order conditions with $[BrONO_2]$ being 4−20 times greater than $[Br]_0$. The temporal variation of NO_3 is given by eq VIII where k' is the first-order rate coefficient for reaction 18 and is equal to $k_{18}[BrONO_2]$. The slope of a plot of k' versus $[BrONO_2]$, Figure 5, yielded $k_{18} = (6.7 \pm 0.7) \times 10^{-11}$ cm^3 $molecule^{-1}$ s^{-1}. The Br atom concentration was varied by a factor of 5 by changing the laser fluence delivered to the cell. No dependence on the initial Br atom concentration was observed.

The rate coefficient for the reaction

$$Cl + BrONO_2 \rightarrow ClBr + NO_3 \qquad (19)$$

was also measured using the same procedures but with Cl_2 substituted for Br_2. Cl_2 concentrations in the range in the range $(1-6) \times 10^{14}$ molecule cm^{-3} were used. The results of these measurements are shown in Figure 5. The value of k_{19} obtained

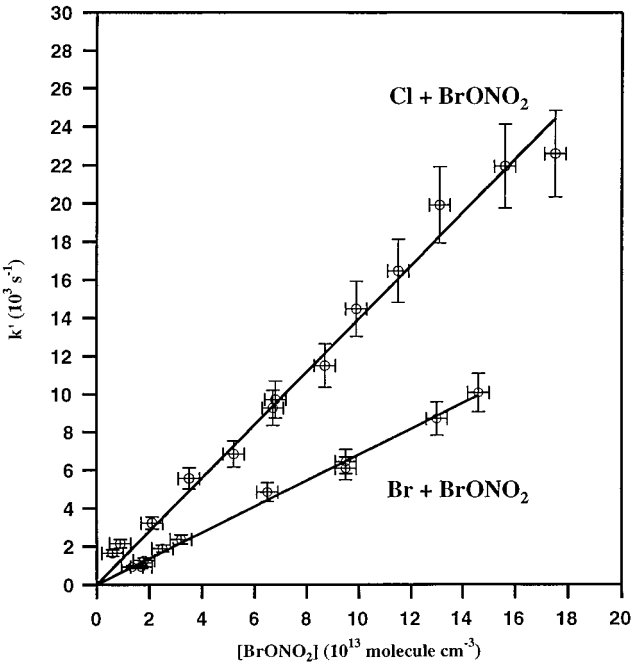

Figure 5. Rate coefficient for the reactions of Br, k_{18}, and Cl, k_{19}, atoms with $BrONO_2$ at 298 K: $k_{18} = (6.7 \pm 0.32) \times 10^{-11}$ cm^3 $molecule^{-1}$ s^{-1} and $k_{19} = (1.27 \pm 0.10) \times 10^{-10}$ cm^3 $molecule^{-1}$ s^{-1}. Quoted uncertainties are 2σ precision of the fits.

is $(1.27 \pm 0.16) \times 10^{-10}$ cm^3 $molecule^{-1}$ s^{-1}. This value has been corrected, 8%, to account for contributions of the loss of Cl atoms via the Cl + Br_2 reaction (1.5×10^{-10} cm^3 $molecule^{-1}$ s^{-1} [15]) to the Cl atom loss.

Using N_2O_5 photolysis for the laser fluence calibration, the NO_3 yield in reactions 18 and 19, Table 5, were found to be 0.88 ± 0.04 and 1.04 ± 0.12, respectively.

The value of k_{14}, the rate coefficient for the reaction of photoproduct X with $BrONO_2$, was determined in the quantum yield measurements in both N_2 and O_2 carrier gases at various pressures. The rate coefficients were found to be independent of pressure. There was no statistically significant difference in the measured rate coefficient with photolysis wavelength; k_{14}= (5.9 ± 2.2), (5.5 ± 2.6), and $(6.4 \pm 1.4) \times 10^{-11}$ cm^3 $molecule^{-1}$ s^{-1} at 248, 308, and 352.5 nm, respectively. The rate coefficients measured in N_2 are perhaps slightly lower, $(5.8 \pm 2.0) \times 10^{-11}$ cm^3 $molecule^{-1}$ s^{-1}, than those measured in O_2, $(6.4 \pm 1.4) \times 10^{-11}$ cm^3 $molecule^{-1}$ s^{-1}.

Error Analysis. The main sources of uncertainty in these measurements arise from (1) the uncertainties in the quantum yield for NO_3 production in N_2O_5 photolysis (estimated to be ∼15% for all wavelengths), (2) the uncertainties in the absorption cross sections of N_2O_5 and $BrONO_2$, (3) the stability of the $BrONO_2$ concentration during the course of the measurement (10%), and (4) the accuracy of the determined NO_3 absorption, $\Delta A_P(NO_3)$ (5% at 248 nm increasing to 20% at 352.5 nm). The latter two uncertainties are reduced by repeated measurements and are included in the precision of the measurements. The first two represent sources of systematic uncertainties. The absolute uncertainty in the quantum yield of NO_3 in $BrONO_2$ is estimated by propagation of errors to be 30, 35, and 45% (2σ, including estimated systematic errors) at 248, 308, and 352.5, respectively.

Discussion

NO_3 Quantum Yields in N_2O_5 Photolysis. Our measured quantum yields for NO_3 production from N_2O_5 photolysis are

TABLE 5: NO_3 Product Yield in the Reactions Br and Cl + $BrONO_2$

$[BrONO_2]^a$ (10^{13})	$[Br_2]$ (10^{15})	$[Br]_0{}^b$ (10^{12})	$[Cl_2]$ (10^{14})	$[Cl]_0{}^b$ (10^{12})	$[NO_3]_0$ (10^{12})	NO_3 yield
1.7			5.6	7.38	6.45	0.87
3.0			2.4	3.16	3.56	1.12
5.4			2.1	2.77	3.12	1.12
5.7			3.5	4.61	4.86	1.05
					average = 1.04 ± 0.12	
6.1	3.5	11.2			9.26	0.83
5.8	2.8	8.95			7.78	0.87
5.8	2.6	8.31			7.72	0.93
3.7	2.3	7.35			6.59	0.90
					average = 0.88 ± 0.04	

[a] Concentrations are in units of molecule cm^{-3}. [b] Concentration was calculated using laser fluence determined in N_2O_5 photolysis experiments to be 3.64×10^{16} photon cm^{-2} $pulse^{-1}$.

in reasonable agreement with previous studies. At 248 nm, we measured $\Phi_\lambda^{NO_3}(N_2O_5) = 0.64 \pm 0.20$ (2σ), which compares well with 0.77 ± 0.13 (2σ) measured by Ravishankara et al.[16] at 248 nm and 0.80 by Burrows et al.[17] at 254 nm. We have corrected these previously reported values using the recent NO_3 absorption cross section data of Yokelson et al.,[6] which was used in our study. The agreement between these quantum yield measurements lies within the 2σ uncertainties.

The NO_3 quantum yield was determined by using both HNO_3 photolysis and F + HNO_3 as actinometeric standards. These two methods agreed to better than 5%. This level of agreement not only gives us confidence in our measurements but also confirms the OH quantum yield value of 1, reported by Turnipseed et al.[18] for HNO_3 photolysis at 248 nm. The yield of NO_3 being less than unity suggests another set of photolysis products. Ravishankara et al.[16] reported the quantum yield for $O(^3P)$ at 248 nm to be 0.72 ± 0.17. The approximate equality between the quantum yields for NO_3 and $O(^3P)$ does not mean that they are produced in the same process. Oh et al.[19] suggested that NO_3 and vibrationally excited NO_2 are products of N_2O_5 dissociation and that NO_2 dissociates further to give NO + O. The possibility of vibrationally excited NO_3 dissociating to NO_2 + O or NO + O_2 must also be considered. Determination of the quantum yields for NO_2 and NO would be very beneficial. Also, studies of N_2O_5 dissociation under collision free conditions would be useful in elucidating the various primary photolysis products.

The quantum yield for NO_3 from N_2O_5 photolysis has not been previously reported at 308 nm. At 350 nm, Swanson et al.[20] quote a N_2O_5 quantum yield that is "close to unity", in reasonable agreement with our average value of 1.03 ± 0.15 at 352.5 nm. Our value of unity at 308 nm substantiates the currently assumed unity value in atmospheric model calculations.

We have used our values of the NO_3 quantum yields in N_2O_5 photolysis for the evaluation of the NO_3 yields from $BrONO_2$.

$BrONO_2$ Quantum Yields. *248 nm.* The measured quantum yield for channel 1b at 248 nm is 0.28 ± 0.09, independent of pressure. Therefore, other primary photolysis products must be produced at this wavelength. Indeed, BrO was observed to be a primary photolysis product. The amount of photolytically produced BrO was approximately 1.8 ± 0.7 times the amount of NO_3 such that the quantum yield for BrO, $\Phi(BrO) \approx 0.5$.

The rise in the NO_3 signal following the photolytic production is a clear indication of the generation of species that react with $BrONO_2$. These reactive species must be either Br or O atoms. The rate coefficient for the NO_3 rise is consistent with generation of Br or a combination of Br and O. The total yield of NO_3, channel 1b and reaction 14, was ~1. Therefore, the sum of the quantum yields of Br and O must be ~0.7. The rate coefficient for the reaction

$$O + BrONO_2 \rightarrow BrO + NO_3 \quad (20a)$$

$$\rightarrow \text{products} \quad (20b)$$

is 3.8×10^{-11} cm^3 $molecule^{-1}$ s^{-1} at 298 K.[21] This is lower than the average measured value of k_{14}, suggesting that the NO_3 rise cannot be due exclusively to O atoms.

The total NO_3 yield (channel 1b and reaction 14) was determined to be 1.12 ± 0.11 in N_2 and 0.91 ± 0.18 in excess O_2. The difference, if it exists, between the N_2 and O_2 carrier gases may suggest that O atoms are produced in the photolysis of $BrONO_2$ with a yield of ~0.2 through either channels 1d, 1e, or 1f. This value is also consistent with the value of k_{14} being slightly lower than that for k_{18}. Such O atom production is similar to that seen in $ClONO_2$ photolysis[22] where an excited NO_2 and/or NO_3 photofragment dissociates yielding an O atom. In any case, the O atom yield is small, less than 0.2. Therefore, we suggest that the yield of Br atom is ~0.5. This is consistent with an estimated BrO quantum yield of 0.5. If the quantum yields for BrO and Br are both 0.5, it is unlikely that species such as $BrNO_2$ or BrONO are produced. A unique analysis of the various $BrONO_2$ photolysis channels is difficult. Direct measurements of the Br atom yield would be helpful.

308 nm. The quantum yield for channel (1b) was determined to be 1.01 ± 0.35 at 308 nm, independent of pressure. However, $\Phi_\infty(NO_3)$ varied between 2.6 and 3. This value of $\Phi_\infty(NO_3)$ is greater than 2, which is the value expected because each Br atom produced in channel 1b should yield another NO_3 through reaction 18. We attribute the larger value of $\Phi_\infty(NO_3)$ to Br_2O photolysis at 308 nm, leading to further production of NO_3 through reactions 18 and 19. An upper limit for the production of BrO from $BrONO_2$ photolysis, reaction 1a, of 0.27 was obtained. However, this value is expected to contain a significant contribution from Br_2O photolysis, reaction 15a. The large value of the quantum yield for NO_3 suggests that channel (1b) is the dominant pathway. However, we cannot exclude other minor channels. Note that the photolysis of the impurities do not affect the quantum yield of NO_3 in $BrONO_2$ photolysis.

352.5 nm. The quantum yield for channel (1b) was determined to be 0.92 ± 0.43 at 352.5 nm. The large uncertainty in the quantum yield reflects the small NO_3 absorption signals and the uncertainty in uniquely distinguishing the photolysis component of the NO_3 from that produced via reaction 14. However, the yields were found to be independent of pressure. The overall NO_3 quantum yield, $\Phi_\infty(1b)$, varied between 2.5 and 4 and was significantly influenced by contributions from Br_2O and Br_2 photolysis. Our results show that the quantum yield for NO_3 is greater than 0.5 but cannot rule out other channels.

Photolysis of $BrONO_2$ appears to be similar to that of $ClONO_2$: at longer wavelengths, the Br−O and Cl−O bonds break. At shorter wavelengths, where energy is available, other products are produced. Also, the photodissociation of both $BrONO_2$ and $ClONO_2$ appear to be prompt at $\lambda < 352$ nm as suggested by the invariance of the quantum yields with pressure of the bath gas.

Kinetics. The rate coefficient, k_{18}, for the reaction of Br with $BrONO_2$ is greater than those obtained from the analysis of the quantum yield data, k_{14}. The ∼20% lower rate coefficients obtained using the quantum yield data can easily be reconciled by contributions to the NO_3 formation rate from reaction 20a where the O atoms could be formed by reactions 1d, 1e, 1f, or 15b. Model simulations with $k_{20a} = 3.8 \times 10^{-11}$ cm^3 molecule^{-1} s^{-1} show that the rate coefficients retrieved from the quantum yield data, k_{14}, depend linearly on the O atom quantum yield. Our values of k_{14} obtained at the different photolysis wavelengths, with and without an O atom scavanger, are consistent with an O atom yield of 10 to 20%. The rate coefficient data, k_{14}, are not accurate enough to distinguish a wavelength dependence to the O atom yield. Wine and co-workers[21] have recently measured k_{18} using a laser flash photolysis−resonance fluorescence technique. Their room temperature value, 6×10^{-11} cm^3 molecule^{-1} s^{-1}, is in reasonable agreement with the value measured in this work.

Atmospheric Implications. Calculations presented by Burkholder et al.[5] showed that for a latitide of 40° N in the summer the average daily photolysis rate for $BrONO_2$ at 20 km altitude is approximately 1000 s^{-1}. This rate of photolysis does not change drastically with altitude or season. They showed that approximately half of the atmospheric photolysis occurs in the wavelength range 300−360 nm, which is the wavelength range addressed by the quantum yield measurements in this study. Our measured unit quantum yield for the production of NO_3, channel 1b, is essentially unity over this range, albeit with large uncertainty limits. This is inconsistent with the recently revised recommendations for stratospheric modeling by DeMore et al.[9] which quote yields for channel 1a of 0.71 and channel 1b of 0.29. On the basis of our NO_3 yields, the direct production of NO appears to be small, if not zero. Therefore, atmospheric ozone loss as a result of $BrONO_2$ photolysis will likely occur through the mechanism involving the photolysis of the NO_3 photoproduct. The remaining component of atmospheric $BrONO_2$ photolysis occurs at wavelengths greater than 360 nm, where quantum yields are not known. At wavelengths greater than 360 nm the $BrONO_2$ absorption spectrum shows several weak electronic transitions (possibly involving excited triplet states). These excited states may be quenched (collisionally and via intersystem crossing). Such relaxation processes could lead to absolute quantum yields of less than one. Even if this were to occur, the photolytic loss rate of $BrONO_2$ would be reduced at most by a factor of 2. However, until direct measurements in this wavelength region become available, we recommend the use of a unit quantum yield for NO_3 production independent of pressure throughout the entire actinic region.

Acknowledgment. M.H. thanks CIRES for the award of a Visiting Fellowship. This work was funded in part by NASA's Upper Atmospheric Research Program. We thank R. Soller, M. Nicovich, and P. Wine for providing their O + $BrONO_2$ rate coefficient data prior to publication.

References and Notes

(1) Friedl, R. R.; Sander, S. P. *J. Phys. Chem.* **1989**, *93*, 4756.
(2) Poulet, G.; Pirre, M.; Magain, F.; Ramaroson, R.; Le Bras, G. *Geophys. Res. Lett.* **1992**, *19*, 2305.
(3) Davis, H. F.; Kim, B.; Johnston, H. S.; Lee, Y. T. *J. Phys. Chem.* **1993**, *97*, 2172.
(4) Orlando, J. J.; Tyndall, G. S.; Moortgat, G. K.; Calvert, J. G. *J. Phys. Chem.* **1993**, *97*, 10996.
(5) Burkholder, J. B.; Ravishankara, A. R.; Solomon, S. *J. Geophys. Res.* **1995**, *100*, 16793.
(6) Yokelson, R. J.; Burkholder, J. B.; Fox, R. W.; Talukdar, R. K.; Ravishankara, A. R. *J. Phys. Chem.* **1994**, *98*, 13144.
(7) Spencer, J. E.; Rowland, F. S. *J. Phys. Chem.* **1978**, *82*, 7.
(8) Harwood: M. H.; Jones, R. L.; Cox, R. A.; Lutman, E.; Rattigan, O. V. *J. Photochem. Photobiol.* **1993**, *A73*, 167.
(9) DeMore, W. B.; Sander, S. P.; Goldan, D. M.; Hampson, R. F.; Kurylo, M. J.; Howard, C. J.; Ravishankara, A. R.; Kolb, C. E.; Molina, M. J. *Chemical Kinetics and Photochemical Data for use in Stratospheric Modeling*; Jet Propulsion Laboratory: Pasadena, CA, 1997; JPL Pub. No. 97-4.
(10) Burkholder, J. B.; Talukdar, R. K.; Ravishankara, A. R.; Solomon, S. *J. Geophys. Res.* **1993**, *98*, 22937.
(11) Maric, D.; Burrows, J. P.; and Moortgat, G. K. *J. Photochem. Photobiol. A: Chem.* **1994**, *83*, 179.
(12) Huey, L. G. Private communication.
(13) Torabi, A. An investigation of the kinetics and excited-state dynamics of the nitrate free radical. Ph.D. Thesis, Georgia Institute of Technology, 1985.
(14) Orlando, J. J.; Burkholder, J. B. *J. Phys. Chem.* **1995**, *99*, 1143.
(15) Nicovich, J. M.; Wine, P. H. *Int. J. Chem. Kinet.* **1990**, *22*, 379.
(16) Ravishankara, A. R.; Wine, P. H.; Smith, C. A.; Barbone, P. E.; Torabi, A. *J. Geophys. Res.* **1986**, *91*, 5355.
(17) Burrows, J. P., Tyndall, G. S.; Moortgat, G. K., 16th Informal Conf. on Photochemistry, Boston, 1984.
(18) Turnipseed, A. A.; Vaghjiani, G. L.; Thompson, J. E.; Ravishankara, A. R. *J. Chem. Phys.* **1992**, *96*, 5887.
(19) Oh, D.; Sisk, W.; Young, A.; Johnston, H. *J. Chem. Phys*. **1986**, *85*, 7146.
(20) Swanson, D.; Kan, B.; Johnston, H. S. *J. Phys. Chem.* **1984**, *88*, 3115.
(21) Soller, R.; Nicovich, J. M.; Wine, P. H. Private communication.
(22) Goldfarb, L.; Schmoltner, A.-M.; Gilles, M. K.; Burkholder, J. B.; Ravishankara, A. R. *J. Phys. Chem.* **1997**, *101*, 6658.
(23) Yokelson, R. J.; Burkholder, J. B.; Fox, R. W.; Ravishankara, A. R. *J. Phys. Chem.* **1997**, *101*, 6607.